

Neutron matter from chiral two- and three-nucleon calculations up to N³LO

C. Drischler,^{1,2,*} A. Carbone,^{1,2,†} K. Hebeler,^{1,2,‡} and A. Schwenk^{1,2,3,§}

¹*Institut für Kernphysik, Technische Universität Darmstadt, 64289 Darmstadt, Germany*

²*ExtreMe Matter Institute EMMI, GSI Helmholtzzentrum für Schwerionenforschung GmbH, 64291 Darmstadt, Germany*

³*Max-Planck-Institut für Kernphysik, Saupfercheckweg 1, 69117 Heidelberg, Germany*

Neutron matter is an ideal laboratory for nuclear interactions derived from chiral effective field theory since all contributions are predicted up to next-to-next-to-next-to-leading order (N³LO) in the chiral expansion. By making use of recent advances in the partial-wave decomposition of three-nucleon (3N) forces, we include for the first time N³LO 3N interactions in many-body perturbation theory (MBPT) up to third order and in self-consistent Green's function theory (SCGF). Using these two complementary many-body frameworks we provide improved predictions for the equation of state of neutron matter at zero temperature and also analyze systematically the many-body convergence for different chiral EFT interactions. Furthermore, we present an extension of the normal-ordering framework to finite temperatures. These developments open the way to improved calculations of neutron-rich matter including estimates of theoretical uncertainties for astrophysical applications.

PACS numbers: 21.65.Cd, 21.30.-x, 21.60.Jz, 26.60.Kp

I. INTRODUCTION

Progress in chiral effective field theory (EFT) for nuclear forces [1, 2] and advances in many-body theory [3–10] offers new paths to systematically improvable calculations of nuclear many-body systems [11, 12]. In recent years infinite nuclear matter has been studied based on chiral EFT interactions within various frameworks like many-body perturbation theory (MBPT) [13–16], in-medium chiral perturbation theory [17], self-consistent Green's function (SCGF) framework [18], coupled-cluster theory [19], the Brueckner-Hartree-Fock approach [20, 21] and Quantum Monte Carlo methods [22–25].

So far, the employed chiral EFT nucleon-nucleon (NN) and three-nucleon (3N) interactions in these calculations were all derived within Weinberg's power counting scheme [1, 2]. Here the leading 3N forces appear at next-to-next-to-leading order (N²LO) and contain two unknown low-energy couplings, c_D and c_E , which need to be determined by fits to few- or many-body observables. In contrast, subleading 3N forces at N³LO do not contain any new low-energy couplings [26, 27] and are thus completely predicted. Hence, including these contributions in calculations offers the possibility to probe systematically the validity of chiral power counting in nuclear systems and to provide estimates of theoretical uncertainties.

Full N³LO calculations of neutron matter were first performed in Refs. [28, 29]. These works showed that 3N forces at N³LO provide surprisingly large contributions to the equation of state especially in symmetric matter. Similar results were found for few-body systems in Ref. [30]. These findings raise fundamental questions concerning the

convergence of the chiral expansion for 3N forces within the employed regularization and power counting scheme.

Generally, the treatment and inclusion of 3N forces is still a challenge in many-body calculations. In particular, due to the complexity and rich analytical structure of 3N forces at N³LO [26, 27] so far it was possible to include effects from 3N interactions only at the Hartree-Fock level in Refs. [28, 29]. While this approximation is expected to be reliable for neutron matter, higher-order terms in the many-body expansion are expected to become significant as soon as the proton fraction becomes sufficiently large. In the present paper we address this issue by making use of two recent advances: a) the development of a novel framework that makes it possible to compute matrix elements of 3N interactions in a partial-wave momentum basis [30] and the availability of matrix elements up to N³LO and large model spaces, and b) the development of a novel normal-ordering framework based on partial-wave matrix elements [16] that allows to systematically include these 3N interactions in calculations of nuclear matter for arbitrary isospin asymmetry. By combining these two advances it is now possible to include general 3N forces that are available in form of plane-wave partial-wave matrix elements and to treat 3N forces on the same footing as NN forces in the many-body expansion. Furthermore, these developments play an important role in view of future calculations that will employ simultaneous evolution of NN and 3N interactions in a momentum basis via similarity renormalization group techniques [31, 32].

In this paper we will exploit and combine these new capabilities and perform improved calculations of neutron matter up to N³LO in MBPT and SCGF. We benchmark results of these two complementary many-body framework against each other and present a generalization of the normal-ordering framework to finite temperatures. The extension of the present N³LO calculations to arbitrary proton fractions is in principle straightforward but requires reliable fit values for the low-energy couplings c_D and c_E at this order [33, 34]. This is work in progress. In

* Email: christian.drischler@physik.tu-darmstadt.de

† Email: arianna@theorie.ikp.physik.tu-darmstadt.de

‡ Email: kai.hebeler@physik.tu-darmstadt.de

§ Email: schwenk@physik.tu-darmstadt.de

neutron matter these short-range and mid-range topologies do not contribute within the employed regularization scheme.

The paper is organized as follows. In Sec. II we specify the set of employed chiral EFT Hamiltonians and describe the novel normal-ordering framework that allows to include general 3N interactions in calculations of nuclear matter. In addition we briefly discuss the many-body frameworks we used for our calculations. In Sec. III we present our results based on three different sets of Hamiltonians, with a special focus on the effects of 3N forces beyond the Hartree-Fock approximation. Furthermore, we analyze the many-body convergence in MBPT by comparing with SCGF results. Finally we present a generalization of our normal-ordering framework to finite temperatures and benchmark results for the energy against exact Hartree-Fock results. In Sec. IV we conclude with a summary and an outlook.

II. CALCULATIONAL DETAILS

A. Chiral EFT Hamiltonians

We consider unevolved NN and 3N forces up to N³LO and calculate the energy per particle of infinite neutron matter in the frameworks of MBPT and SCGF. The Hamiltonian takes the form

$$H = T + V_{\text{NN}} + V_{\text{3N}} + \dots, \quad (1)$$

where T , V_{NN} and V_{3N} denote the kinetic energy, the NN and 3N interactions, respectively. So far, in most calculations of nuclear matter NN and 3N forces were not included consistently up to the same order in the chiral expansion due to the complex structure of 3N forces at N³LO [26, 27]. Only recently an efficient partial-wave decomposition of these contributions was developed in Ref. [30]. In Refs. [28, 29] the N³LO 3N contributions were evaluated exactly for neutron matter and symmetric nuclear matter in Hartree-Fock approximation. It was somewhat unexpected that the subleading 3N forces provide significant contributions to the energy. The findings suggest that it is mandatory to investigate these contributions more systematically by including higher-order effects in the many-body expansion.

We note that, considering only NN and 3N forces at N³LO in Eq. (1) is still not fully consistent in the chiral expansion. In fact, four-nucleon (4N) forces also contribute at this order. However, Ref. [28, 29, 35] demonstrated that the 4N contributions to the energy in neutron matter in the Hartree-Fock approximation are very small compared to the overall uncertainty, $E_{4\text{N}}/N \sim -180$ keV at saturation density. Therefore, 4N contributions only lead to a small shift for all Hamiltonians and do not affect the relative comparison of MBPT and SCGF. Consequently, if not stated otherwise, we neglect 4N (and higher-body) contributions in Hamiltonian (1) and focus on the improvement of subleading 3N forces.

Normal-ordering with respect to a reference state is a well-known method to include 3N contributions in terms of density-dependent effective NN forces, which can then be directly included in NN frameworks. Usually, the remaining residual 3N Hamiltonian leads to small contributions in pure neutron matter and is thus neglected (see, e.g., Ref. [19]). Following Refs. [36, 37] we obtain the effective NN interaction $\bar{V}_{\text{3N}}^{\text{as}}$ by summing one particle over the occupied states of the reference state, i.e.,

$$\bar{V}_{\text{3N}}^{\text{as}} = \text{Tr}_{\sigma_3} \int \frac{d\mathbf{k}_3}{(2\pi)^3} \mathcal{A}_{123} V_{\text{3N}} n_{\mathbf{k}_3} \Big|_{\text{nnn}}, \quad (2)$$

with the momentum-distribution function $n_{\mathbf{k}}$ and \mathcal{A}_{123} is the antisymmetrizer. At zero temperature it is common to approximate the distribution function by the free Fermi gas function $n_{\mathbf{k}} = \Theta(k_{\text{F}} - |\mathbf{k}|)$, with Fermi momentum k_{F} . It was demonstrated that the inclusion of correlations in the reference state leads to small effects in observables [38]. In this article, we also discuss the extension of the normal-ordering framework to finite temperatures.

The 3N interactions V_{3N} are regularized using non-local regulators of the form $f_{\text{R}}(p, q) = \exp[-((p^2 + 3q^2/4)/\Lambda_{\text{3N}}^2)^4]$ with respect to the Jacobi momenta p, q . In the literature, Eq. (2) has been first evaluated directly based on the operatorial form of the 3N forces at N²LO [13, 36, 37]. Since this procedure becomes rather involved for subleading 3N forces, so far only leading 3N interactions could be considered in this approach. One way to solve this is to make use of the recently developed partial-wave decomposition of the 3N interactions [30] and evaluate Eq. (2) in a partial-wave momentum basis of the form

$$|pq\alpha\rangle \equiv |pq; \left[(LS)J \left(l \frac{1}{2} \right) j \right] \mathcal{J} \left(T \frac{1}{2} \right) \mathcal{T} \rangle. \quad (3)$$

The quantum numbers L , S , J , and $T = 1$ (for neutron matter) denote the relative orbital angular momentum, spin, total angular momentum, and isospin of particles 1 and 2 with relative momentum p . The quantum numbers l and j , respectively, are the orbital angular momentum and total angular momentum of particle 3 relative to the center of mass of the pair with relative momentum p . The quantum numbers \mathcal{J} and $\mathcal{T} = 3/2$ define the total 3N angular momentum and isospin. The 3N matrix elements are provided by Ref. [30] with total three- and two-body quantum numbers $\mathcal{J} \leq 9/2$ and $J \leq 6$, respectively. The size of this model space is sufficient to ensure convergence for calculations of nuclear matter in the Hartree-Fock approximation [16, 30] (see also Sec. IIID). The resulting effective NN interaction is then added to the NN interactions:

$$V_{\text{NN}+3\text{N}}^{\text{as}} = V_{\text{NN}}^{\text{as}} + \zeta \bar{V}_{\text{3N}}^{\text{as}}. \quad (4)$$

We refer to Ref. [16, 36, 38] for detailed discussions on the combinatorial normal-ordering factor ζ . We also note that the summation in Eq. (2) results in a dependence

of \bar{V}_{3N}^{as} on the total momentum \mathbf{P} of the two particles, which is not the case for free-space NN forces due to Galilean invariance. This additional momentum makes the effective NN potential (2) computationally involved. Commonly, the approximation $\mathbf{P} = 0$ is applied, e.g., in Ref. [18, 36, 37]. In Ref. [16], an additional approximation that averages over all directions of \mathbf{P} opposed to $\mathbf{P} = 0$ is studied. It is shown that the resulting 3N Hartree-Fock energies are in reasonable agreement in particular below saturation density. Since the dependence on \mathbf{P} is currently not implemented in the SCGF code and since we focus on the benchmark of MBPT to this nonperturbative method we focus here on the $\mathbf{P} = 0$ approximation for \bar{V}_{3N}^{as} . Finally, we note that once reasonable fit values for c_D and c_E are available at N³LO, the described methods can be directly applied beyond neutron matter.

B. Many-body frameworks

We calculate the energy per neutron at zero temperature up to third order in MBPT. The following notation is used to distinguish interaction energies and total energies at a given order in perturbation theory:

$$\frac{E^{(\text{HF})}}{N} = \frac{T}{N} + \frac{E^{(1)}}{N}, \quad (5a)$$

$$\frac{E_{\text{tot}}^{(2)}}{N} = \frac{E^{(\text{HF})}}{N} + \frac{E^{(2)}}{N}, \quad (5b)$$

$$\frac{E_{\text{tot}}^{(3)}}{N} = \frac{E_{\text{tot}}^{(2)}}{N} + \frac{E^{(3)}}{N}. \quad (5c)$$

Particle-hole contributions are neglected at third-order similarly to Refs. [16, 29, 39]. In order to estimate the uncertainties due to neglected higher-order contributions we perform calculations with a free and a Hartree-Fock single-particle spectrum. We refer to Ref. [16, 36] for details of the calculation. We assess the many-body convergence order-by-order by comparing to SCGF. In the SCGF method, the energy per neutron is calculated nonperturbatively via knowledge of a dressed one-body Green's function [40]. The energy is obtained in the so-called ladder approximation, where an infinite sum of particle-particle and hole-hole diagrams is performed [41, 42]. Similar to the MBPT calculations, particle-hole contributions are neglected. The SCGF approach has been recently extended to self-consistently include 3N forces [43]. In this extension, the ladder resummation and the self-energy are redefined incorporating normal-ordered 3N terms with respect to a dressed reference state. Residual 3N contributions are also neglected in this approach. In this extended approach, the modified sum rule to obtain the total energy per particle in neutron matter reads [43]:

$$\frac{E}{N} = \frac{2}{n} \int \frac{d\mathbf{k}}{(2\pi)^3} \int \frac{d\omega}{2\pi} \frac{1}{2} \left\{ \frac{k^2}{2m} + \omega \right\} A(k, \omega) f(\omega) - \frac{\langle W \rangle}{2}, \quad (6)$$

where n the total density of the system and $f(\omega)$ corresponds to the Fermi-Dirac distribution function. $A(k, \omega)$

is the spectral function; this quantity gives the probability of adding or removing a particle with momentum k which causes an excitation in energy $d\omega$ in the many-body system. $\langle W \rangle$ is the expectation value of the 3N operator (see Ref. [38] for details). Throughout the paper we will refer to Eq. (6) as E_{SCGF}/N . The present implementation of SCGF is not capable of treating the appearance of pairing below a critical temperature, for this reason calculations are always performed at finite T . The pairing instability does not affect the MBPT calculations because the energy diagrams are evaluated directly, for which the pairing singularity is integrable. The zero-temperature results in SCGF are extrapolated using the Sommerfeld expansion [41]. In this expansion, the energy can be written as a quadratic expansion in terms of T/ε_F , where ε_F is the Fermi energy, as long as $T/\varepsilon_F \ll 1$. A more sophisticated computational method to numerically extrapolate self-energies, spectral functions and thermodynamical properties from finite to zero temperature has been recently presented in Ref. [44].

In order to extend the effective NN interaction \bar{V}_{3N}^{as} to finite temperatures, we extend the framework presented in Ref. [16] and evaluate Eq. (2) at finite temperature using the general Fermi-Dirac distribution function, $n_{\mathbf{k}} = [\exp(\beta(\varepsilon_{\mathbf{k}} - \mu)) + 1]^{-1}$. Given a total density n , we compute the chemical potential $\mu(n)$ by solving the non-linear density relation

$$n = \frac{1}{\pi^2} \int_0^\infty dk k^2 n_{\mathbf{k}}(\mu). \quad (7)$$

We consider here the free single-particle energy, i.e., $\varepsilon_{\mathbf{k}} = k^2/(2m)$. Higher-order corrections to the self energy include contributions from the effective NN potential itself and would require thus an involved self-consistent solution for the spectrum. It has been shown in Ref. [38] that the energy per particle in pure neutron matter shows only at higher densities a dependence on the momentum distribution used in Eq. (2). Such high densities are not considered in this work, but it will be important to check this approximation at high temperatures.

III. RESULTS

A. Comparison of MBPT and SCGF

We show in Fig. 1 the energy per particle as a function of density in neutron matter at zero temperature. From left to right, the first row shows the results for the N³LO NN potentials EM 500 MeV [45], EGM 450/500 MeV and EGM 450/700 MeV [46] with leading N²LO 3N forces. The momentum scales attached to the potentials correspond to different regulator cutoffs: first, the cutoff in the Lippmann-Schwinger equation and second, if not dimensionally regularized, the cutoff in the two-pion-exchange spectral-function regularization. Analogously, the second

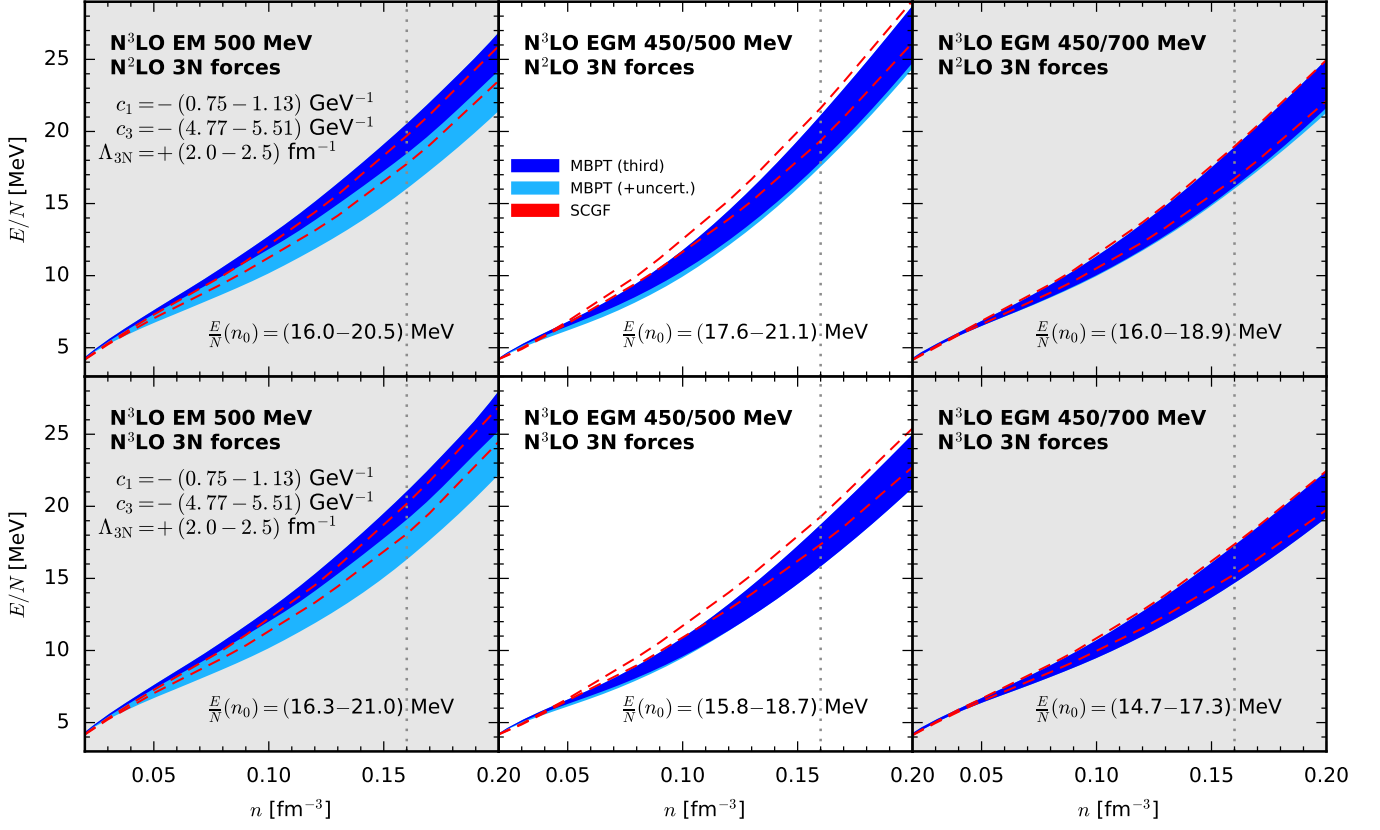


FIG. 1. (Color online) The energy per particle in neutron matter for three different $N^3\text{LO}$ NN potentials with $N^2\text{LO}$ (top) and $N^3\text{LO}$ (bottom) 3N forces, respectively. The uncertainty bands are due to the given c_i and 3N cutoff variation. For the MBPT results, we consider in addition the maximum range of third-order calculations with a free and a Hartree-Fock spectrum (dark-blue band) plus the change from a second-order calculation with a Hartree-Fock spectrum, which is indicated by the light-blue extension of the pure third-order uncertainty band. The two bands together define the total uncertainty estimate of MBPT. The region between the two red-dashed lines denotes the uncertainty band of the SCGF method, which we do not fill for a better view. In each panel the energy range at saturation density obtained in MBPT is given.

row shows the results for the same NN potentials but including 3N forces up to $N^3\text{LO}$. We consider two sources of uncertainties: from the chiral Hamiltonian and from considering only a finite order in MBPT. As stated in Fig. 1, the theoretical uncertainties due to the Hamiltonian are estimated by parameter variation in the 3N forces, i.e., the cutoff Λ_{3N} and the low-energy constants c_1 and c_3 . The c_i values need to be refit at each chiral order, however, to investigate the net effect of $N^3\text{LO}$ forces, we take here solely the c_i -range recommended for $N^3\text{LO}$ calculations [47]. In addition to the uncertainties in the Hamiltonian, we estimate the neglected higher-order contributions in the many-body expansion by varying the single-particle energies at third order using a free and a Hartree-Fock spectrum. These bands are colored in dark blue in Fig. 1. Moreover, following Ref. [29] we include the results at second order in MBPT using a Hartree-Fock spectrum to the uncertainty estimate. This extension of the pure third-order equation of state is indicated by light-blue bands. In summary, for a given Hamiltonian we perform in total three calculations in MBPT: two third-order

calculations using the two single-particle spectra and a second-order calculation using a Hartree-Fock spectrum. Light- and dark-blue bands together characterize the total uncertainty estimate of MBPT in each panel. The actual energy range of MBPT is given in each panel of Fig. 1 at saturation density n_0 (dashed vertical line), with $n_0 = 0.16 \text{ fm}^{-3}$.

Let us focus on the results with leading 3N forces, as shown in the first row of Fig. 1. The qualitative description does not change for the calculations with subleading 3N forces (second row in Fig. 1). Whereas the results for the two EGM potentials are almost independent of the many-body details, the effects of the variation of spectra and many-body order in MBPT are much more pronounced for EM 500 MeV: at saturation density the many-body uncertainties provide contributions of about $\sim -2.5 \text{ MeV}$ for this Hamiltonian (see light-blue band in Fig. 1). Including subleading 3N forces leads basically only to an overall shift of the bands as shown by the given energy range at saturation density. More specifically, the net 3N contribution leads to more attraction

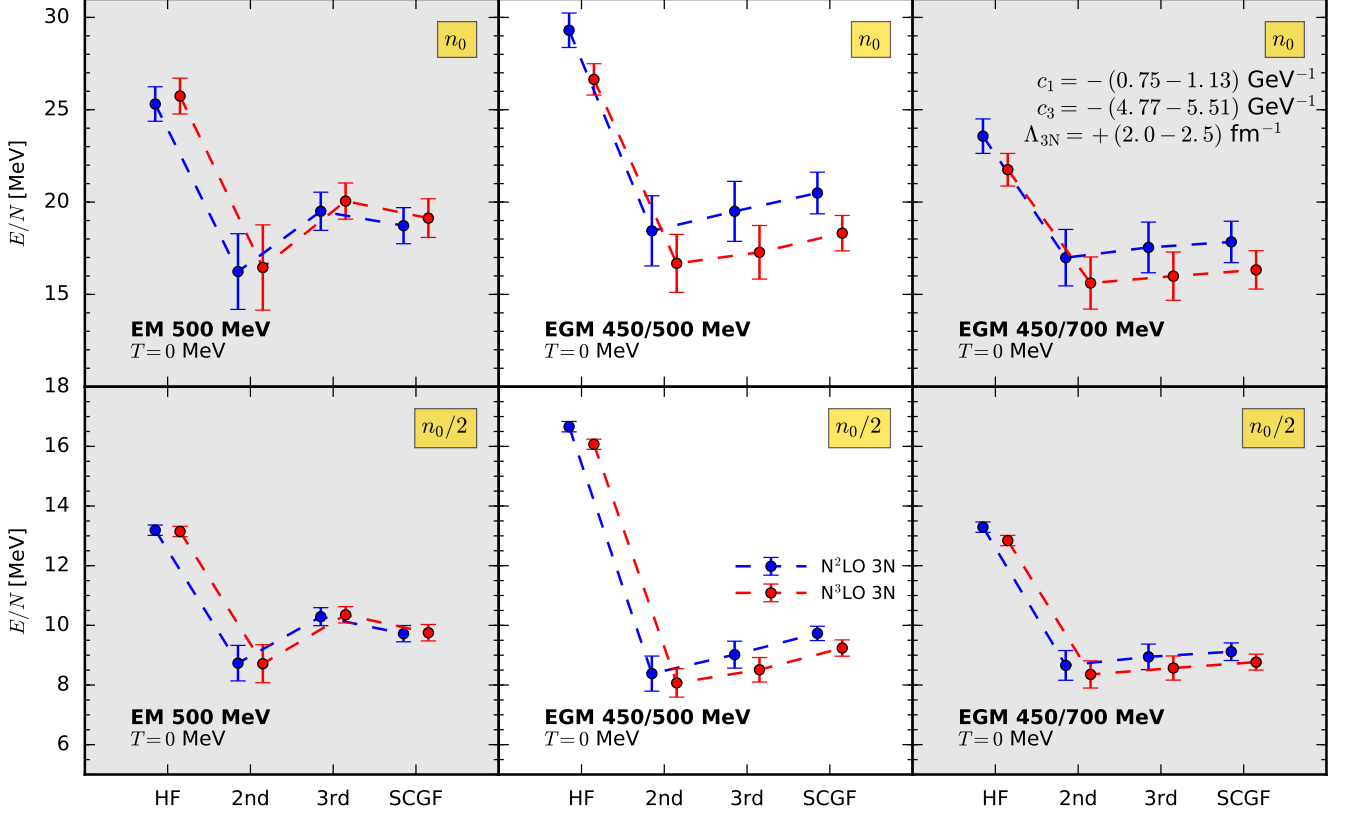


FIG. 2. (Color online) The energy per particle at different orders of MBPT is shown, up to Hartree-Fock ($E_{\text{tot}}^{\text{HF}}/N$), second order ($E_{\text{tot}}^{(2)}/N$) and third order ($E_{\text{tot}}^{(3)}/N$), respectively, in comparison to the energies obtained from the SCGF method (E_{SCGF}/N) at n_0 (first row) and $n_0/2$ (second row), respectively. The N^3 LO NN potentials are given in each panel. Three-body effects are included at N^2 LO (blue) and at N^3 LO (red), respectively. The dashed lines connecting the data points are in order to guide the eyes. The error bars are due to the c_i and Λ_{3N} variations. In this plot, the third-order calculation does not include the additional many-body uncertainty (the light-blue band in Fig. 1).

for the EGM potentials while the effect on EM 500 MeV is slightly repulsive.

To quantify the many-body convergence in more detail we compare to the results obtained in the SCGF method which are given by the region between the red-dashed lines in Fig. 1. The results in SCGF are considered to be converged in the many-body expansion (at the ladder level) and thus include only the uncertainty due to the Hamiltonian (including variations of the low-energy constants c_1, c_3). We focus again on the different NN potentials rather than on discussing the effect of subleading 3N forces. Considering the total uncertainty estimate of MBPT we find for the potentials EM 500 MeV and EGM 450/700 MeV completely overlapping bands and similar trends in density. In the case of EM 500 MeV the extended uncertainty (light-blue band) is however needed to obtain more attraction and consequently fully overlapping bands, whereas for EGM 450/700 MeV the pure third-order energy is already in remarkable agreement. In addition to the above discussion on the size of the light-blue bands this suggests that contributions beyond

third-order are small for EGM 450/700 MeV and become significant for EM 500 MeV.

For EGM 450/500 MeV we observe a slightly different density dependence between the MBPT and the SCGF curves, leading to an almost total overlap at saturation density but less agreement in the region around $n \sim 0.1 \text{ fm}^{-3}$. Here, the equation of state in SCGF is slightly more repulsive. We recall that the SCGF results are extrapolated down to zero temperature from calculations performed at $T = 2 \text{ MeV}$ for $n \leq 0.05 \text{ fm}^{-3}$ and at $T = 5 \text{ MeV}$ for densities above. We have tested whether this discrepancy is related to the extrapolation to zero-temperature lowering the temperature down to $T = 3, 4 \text{ MeV}$ in densities between 0.05 and 0.10 fm^{-3} , and have found no dependency on the extrapolation.

Combining the discussions on the size of the additional many-body uncertainty and the comparison of MBPT vs. SCGF we conclude from Fig. 1 that the perturbativeness improves from EM 500 MeV to EGM 450/500 MeV to EGM 450/700 MeV. It is remarkable that a third-order MBPT calculation compares so well with the nonpertur-

bative case for these chiral NN potentials. We study the many-body convergence as well as the effect of subleading 3N forces in more details in the next section.

B. Many-body convergence

In Fig. 2 we address again the many-body convergence and show order-by-order in MBPT the total energy per neutron at n_0 (first row) and $n_0/2$ (second row), analogously to Fig. 1. More specifically, we show the total energy in Hartree-Fock approximation $E_{\text{tot}}^{(\text{HF})}/N$ (“HF”), second order (“2nd”) and third order (“3rd”), $E_{\text{tot}}^{(2)}/N$ and $E_{\text{tot}}^{(3)}/N$ respectively, in comparison to the results obtained in the SCGF method, E_{SCGF}/N (“SCGF”). The uncertainties are obtained as in Fig. 1 through variations of the 3N parameters and the single-particle energies. However, to study the many-body convergence the third-order bands do not include here the additional many-body uncertainty (the light-blue bands of Fig. 1). The blue (red) data points correspond to $N^2\text{LO}$ ($N^3\text{LO}$) 3N forces.

For all six panels in Fig. 2 we observe similar overall patterns: comparing order-by-order to the SCGF method we observe that the second order adds always too much attraction which then is compensated by the third-order repulsion. However, the specific behavior is different for EM 500 MeV and the two EGM potentials. In the case of EM 500 MeV the large third order overcompensates the second-order repulsion. In contrast, the third-order contribution is much smaller and less repulsive for the EGM potentials as can be seen in Fig. 2 (second and third column). In particular, this is pronounced in the calculations based on EGM 450/700 MeV, which agree remarkably well with the SCGF result.

As already discussed in the description of Fig. 1, including $N^3\text{LO}$ 3N forces has only a small repulsive effect on the energies based on EM 500 MeV, whereas the effect on the EGM potentials is larger but attractive. This behavior can be traced back to NN-3N mixing terms that enter the calculation when including 3N forces beyond the HF level. We also note that the values of the low-energy constants C_S and C_T , which enter $N^3\text{LO}$ 3N contributions, differ for all three potentials. However, the many-body convergence is not altered by including contributions from subleading 3N interactions.

C. Comparison to previous calculations at $N^3\text{LO}$

The authors of Refs. [28, 29] performed the first consistent calculations at $N^3\text{LO}$ including NN, 3N and 4N forces in MBPT. In the cited works $N^3\text{LO}$ NN and $N^2\text{LO}$ 3N forces have been considered up to third order in MBPT in terms of effective NN potentials [36], whereas subleading 3N interactions could only be included in the Hartree-Fock approximation since no 3NF partial-wave matrix elements were available at that time. Thanks to the ad-

vances discussed in this paper we are now in the position to revisit and systematically improve these calculations.

In Fig. 3 we show our improved results for the energy of neutron matter (blue bands) for the three Hamiltonians EM 500 MeV, EGM 450/500 MeV and EGM 450/700 MeV (first row) and the total band merged from the previous panels (second row). The uncertainty bands cover again variations of the 3N parameters (as given in the figure), the single-particle spectrum and the additional many-body uncertainty (see also discussion of Fig. 1). We furthermore include the 4N Hartree-Fock results, as given in Ref. [29], and vary the 4N cutoff analogously to the 3N forces. In addition, we show the results of Ref. [29]¹ depicted by the black solid lines. For a better view we do not fill this region. We give in each panel the energy range at saturation density obtained within the improved calculations presented in this work.

We observe that the effect of adding the $N^3\text{LO}$ 3N contributions beyond Hartree-Fock varies significantly between the EM 500 MeV and the two EGM potentials. For EM 500 MeV these contributions leave the uncertainty band almost unaffected. For the two EGM potentials the upper uncertainty limits remains the same while the lower increase by ~ 1 MeV (~ 0.2 MeV) for EGM 450/500 MeV (EGM 450/700 MeV), hence decreasing the width of the uncertainty band. These findings are consistent with the observations in Ref. [29], which stated that the $N^3\text{LO}$ 3N Hartree-Fock energy is smaller for EM 500 MeV while it is much larger for the two EGM potentials (see Fig. 6 of Ref. [29]). We emphasize, however, that NN and effective NN forces get mixed at second-order and beyond, and therefore the net effect of these subleading 3N contributions cannot be easily disentangled in the many-body calculation. Combining all bands we find a total uncertainty of $\frac{E}{N}(n_0) = (14.7 - 21.1)$ MeV in neutron matter at saturation density. Compared to the corrected total band of Ref. [29] $\frac{E}{N}(n_0) = (14.3 - 21.1)$ MeV, we obtain a slight reduction of the lower limit of the uncertainty band. As suggested in Refs. [28, 29], these effects are indeed rather small. However, we expect the effects to be much more important as soon as the proton fraction is finite (see also discussion of symmetric nuclear matter in Ref. [29]).

D. Normal-ordering at finite temperatures

We have extended the recently-developed framework for computing effective NN potentials in a partial-wave basis [16] to finite temperatures. Besides being a necessary step in order to include these matrix elements in

¹ For completeness, we have corrected a small error in the routines of Ref. [29] for the computation of the second- and third- order contribution of the $N^3\text{LO}$ NN plus $N^2\text{LO}$ 3N forces as well as the $N^3\text{LO}$ 3N Hartree-Fock energy corresponding to the ring topology. Moreover, we are using the typo-corrected values for $\beta_{8,9}$ (see Ref. [48] for details).

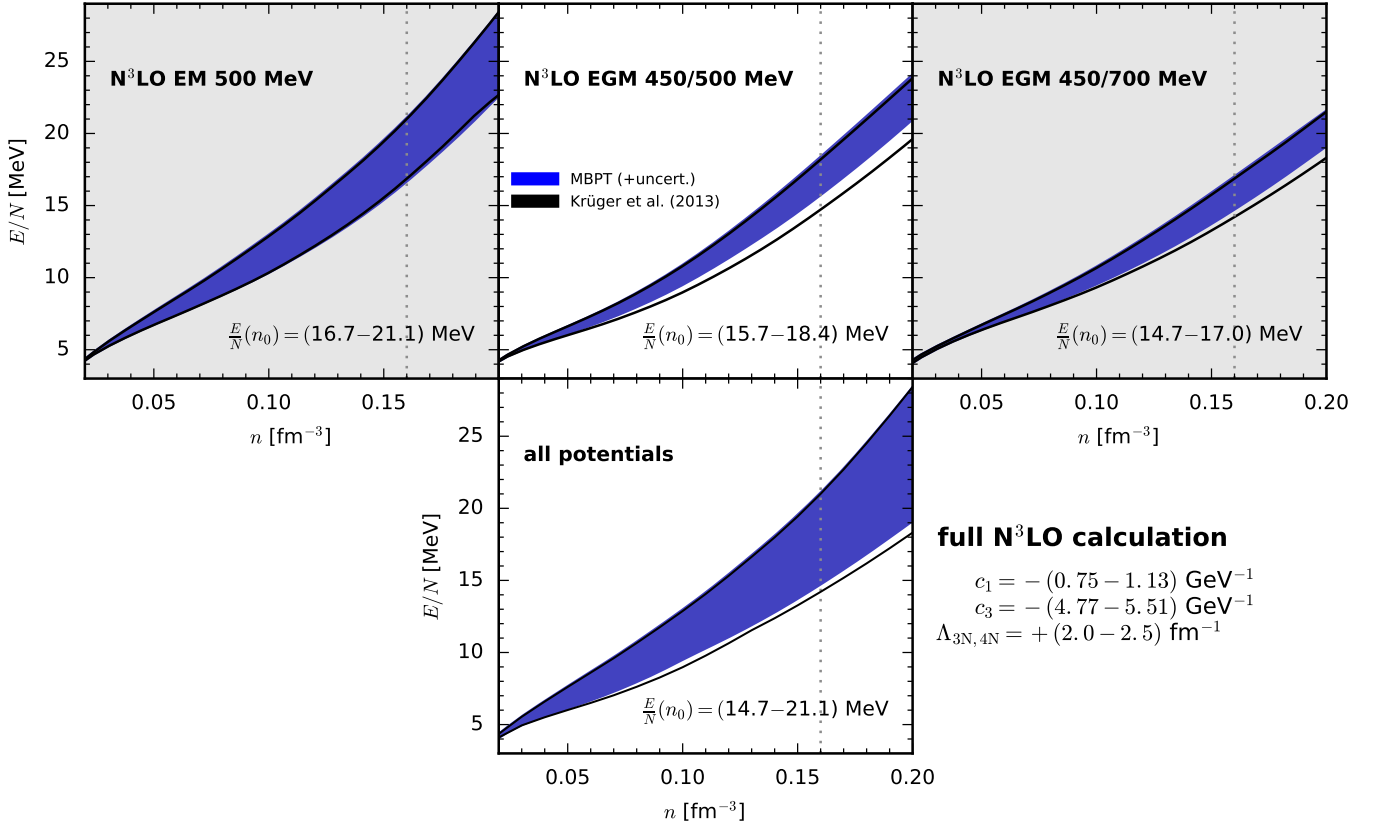


FIG. 3. (Color online) The energy per particle of neutron matter at $N^3\text{LO}$ for the three different NN potentials (this work: blue bands) in comparison to Ref. [29] (Krüger et al. (2013): black lines). The second row combines the results of the first row. In each panel, we give the energy range at saturation density obtained within the improved calculations presented in this work. See text for details.

the SCGF method (due to the extrapolation from finite temperatures), this is also a crucial step for future MBPT calculations of nuclear matter at finite temperatures. In Fig. 4 we show the resulting $N^2\text{LO}$ 3N Hartree-Fock energies $E^{(1)}/N(n_0, T)$ at six different temperatures in the range of $T = (0-50)$ MeV. We benchmark our new values (red) against previous results (blue) obtained via an operatorial approach [38]. The uncertainty bands are obtained through 3N parameter variation analogously to Figs. 1 and 2. The single-particle spectrum does not contribute to the uncertainties since the Fermi-Dirac distribution in Eq. (2) is computed using a free spectrum. A similar benchmark at $N^3\text{LO}$ is not possible since no matrix elements are currently available based on the operatorial evaluation of 3N forces at $N^3\text{LO}$. We note that the 3N interaction energy decreases with temperature as shown in Fig. 4. Including also kinetic energy contributions would lead to a total increase in energy with increasing temperature. From Fig. 4 we can conclude that the two different methods for the normal-ordering agree very well at zero and finite temperature up to $T = 50$ MeV.

In addition to the 3N Hartree-Fock energies, we also benchmark the underlying interaction matrix elements

of the effective potential \bar{V}_{3N}^{as} . The results for a selection of four partial-wave channels and two temperatures are shown in Fig. 5. These matrix elements contribute to the energy presented in Fig. 4. The ones obtained in the partial-wave (operatorial) approach are plotted as dashed (solid) lines. We select a representative set of channels, 1S_0 , 3P_0 , 3P_1 , and 3P_2 , and temperatures $T = 10, 50$ MeV. We have also compared higher partial waves up to $J = 6$ and momentum off-diagonal matrix elements for $\Lambda_{3N} = (2.0 - 2.5) \text{ fm}^{-1}$. As in Ref. [16], we find indications of an incomplete partial-wave convergence only for partial-waves channels with $J > 4$. We also checked that the agreement can be systematically improved by increasing the 3N model space, i.e. by including channels with $\mathcal{J} = 11/2$ and $13/2$. We found that contributions from these higher partial-wave channels provide $\lesssim 50$ keV to the energy of neutron matter per particle at saturation density. Overall, we find excellent agreement of the two methods at the level of matrix elements and at finite-temperatures. This shows that the computed matrix elements of the effective interactions at finite temperature at $N^2\text{LO}$ and $N^3\text{LO}$ are correct and numerically stable

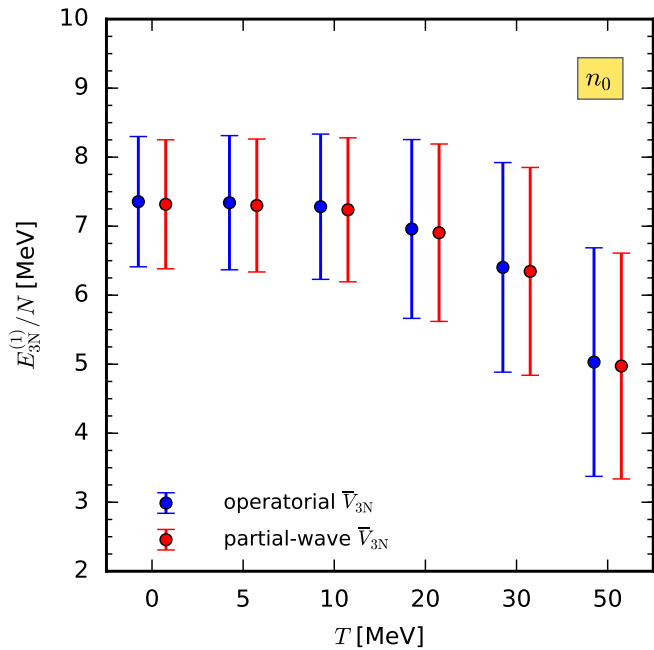


FIG. 4. (Color online) Comparison of the leading 3N Hartree-Fock energies at saturation density for several temperatures obtained using the effective NN potential in terms of 3N operators (blue) and the partial-wave approach (red). We include 3N matrix elements up to $\mathcal{J} \leq 9/2$ and $J \leq 6$. For the uncertainty estimate we use the same parameter variation in the 3N forces as in Fig. 1.

and are hence suitable for future calculations of nuclear matter for astrophysical applications [49].

IV. SUMMARY AND OUTLOOK

In this work we have calculated the zero-temperature equation of state of neutron matter in the framework of MBPT and SCGF based on chiral NN and 3N forces up to $N^3\text{LO}$. In addition, we included contributions from 4N interactions at $N^3\text{LO}$ in the Hartree-Fock approximation. For the inclusion of 3N interactions we have utilized our generalized normal-ordering framework first presented in Ref. [16]. We demonstrated that this framework is able to treat general 3N interactions that are provided in a partial-wave representation and can be extended to finite temperatures.

We have systematically improved previous calculations of neutron matter in MBPT at $N^3\text{LO}$ [28, 29] by including subleading 3N contributions beyond the Hartree-Fock approximation. Specifically, we have obtained the neutron-matter energy based on three different NN plus 3N interactions derived within chiral EFT, comparing calculations including only leading to up-to-subleading 3N forces. For the $N^3\text{LO}$ NN potentials EGM 450/500 MeV and EGM 450/700 MeV we found additional attractive subleading 3N contributions of about ~ 2 MeV for the

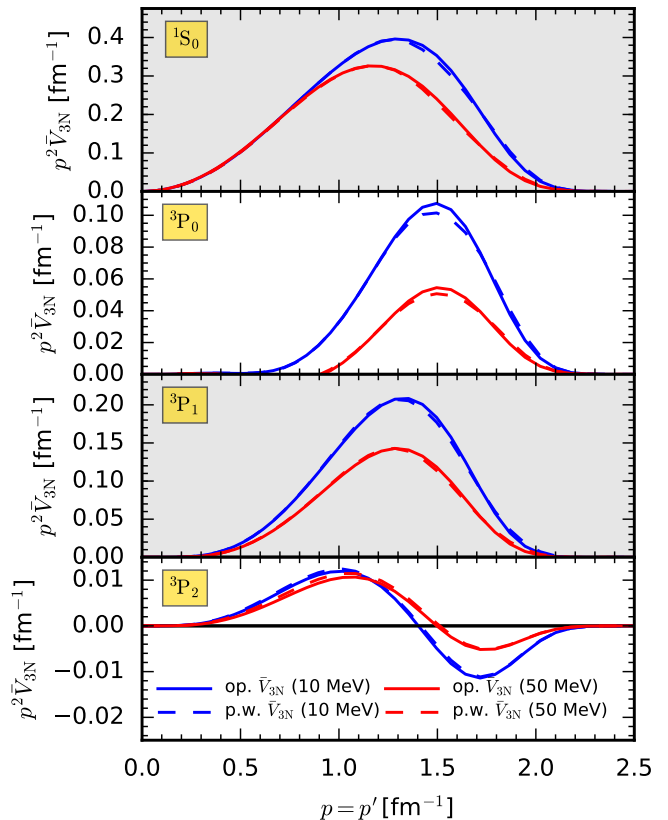


FIG. 5. (Color online) Momentum-space diagonal matrix elements of the density-dependent effective NN potentials at $N^2\text{LO}$ for a selection of four partial-wave channels and two temperatures.

energy per particle at saturation density, while for the EM 500 MeV potential these contributions are smaller in size and repulsive, of the order of ~ 500 keV. In order to assess the many-body convergence we have benchmarked our MBPT results for three commonly-used $N^3\text{LO}$ NN potentials plus leading and also subleading 3N forces against results obtained within the SCGF framework. Since the current implementation of SCGF does not account for Cooper pairing, the zero-temperature limit was obtained by extrapolation. We found a systematic convergence of the MBPT results to the SCGF results at third order in MBPT, whereas the detailed convergence pattern depends on details of the NN and 3N interactions.

Finally, we have successfully benchmarked results for the effective NN potential at finite temperature. At order $N^2\text{LO}$ in the chiral expansion we obtain excellent agreement between results obtained using our novel normal-ordering framework and previous results for 3N Hartree-Fock energy contributions as well as on the level of partial-wave matrix elements. These benchmarks demonstrate that we are now in the position to perform calculations of general isospin-asymmetric matter including all NN and 3N contributions up to $N^3\text{LO}$ at zero and finite temperatures. Since all 3N topologies contribute for these

systems, reliable fits of the 3N low-energy constants c_D and c_E are required. This is currently work in progress. The availability of different sets of Hamiltonians using different regulator choices (see also Refs. [50, 51]) and different fitting strategies (see, e.g., Refs. [52, 53]) will make it possible to probe systematically the order-by-order convergence in the chiral expansion. In turn, this will advance our understanding of the dense matter equation of state.

ACKNOWLEDGMENTS

We thank T. Krüger, A. Rios, A. Polls and I. Tews for useful discussions. This work was supported by the ERC Grant No. 307986 STRONGINT, the Deutsche Forschungsgemeinschaft through Grant SFB 1245. A.C. acknowledges support by the Alexander von Humboldt Foundation through a Humboldt Research Fellowship for Postdoctoral Researchers.

-
- [1] E. Epelbaum, H.-W. Hammer, and U.-G. Meißner, *Rev. Mod. Phys.* **81**, 1773 (2009).
 - [2] R. Machleidt and D. R. Entem, *Phys. Rept.* **503**, 1 (2011).
 - [3] V. Somà, A. Cipollone, C. Barbieri, P. Navrátil, and T. Duguet, *Phys. Rev. C* **89**, 061301(R) (2014).
 - [4] S. Binder, J. Langhammer, A. Calci, and R. Roth, *Phys. Lett. B* **736**, 119 (2014).
 - [5] J. D. Holt, J. Menéndez, J. Simonis, and A. Schwenk, *Phys. Rev. C* **90**, 024312 (2014).
 - [6] T. A. Lähde, E. Epelbaum, H. Krebs, D. Lee, U.-G. Meiner, and G. Rupak, *Phys. Lett. B* **732**, 110 (2014).
 - [7] G. Hagen, T. Papenbrock, M. Hjorth-Jensen, and D. J. Dean, *Rept. Prog. Phys.* **77**, 096302 (2014).
 - [8] A. Signoracci, T. Duguet, G. Hagen, and G. Jansen, *Phys. Rev. C* **91**, 064320 (2015).
 - [9] E. Dikmen, A. F. Lisetski, B. R. Barrett, P. Maris, A. M. Shirokov, and J. P. Vary, *Phys. Rev. C* **91**, 064301 (2015).
 - [10] H. Hergert, S. K. Bogner, T. D. Morris, A. Schwenk, and K. Tsukiyama, *Phys. Rept.* **621**, 165 (2016).
 - [11] H.-W. Hammer, A. Nogga, and A. Schwenk, *Rev. Mod. Phys.* **85**, 197 (2013).
 - [12] K. Hebeler, J. D. Holt, J. Menéndez, and A. Schwenk, *Annu. Rev. Nucl. Part. Sci.* **65**, 457 (2015).
 - [13] K. Hebeler, S. K. Bogner, R. J. Furnstahl, A. Nogga, and A. Schwenk, *Phys. Rev. C* **83**, 031301(R) (2011).
 - [14] L. Coraggio, J. W. Holt, N. Itaco, R. Machleidt, L. E. Marcucci, and F. Sammarruca, *Phys. Rev. C* **89**, 044321 (2014).
 - [15] C. Wellenhofer, J. W. Holt, N. Kaiser, and W. Weise, *Phys. Rev. C* **89**, 064009 (2014).
 - [16] C. Drischler, K. Hebeler, and A. Schwenk, *Phys. Rev. C* **93**, 054314 (2016).
 - [17] J. W. Holt, N. Kaiser, and W. Weise, *Prog. Part. Nucl. Phys.* **73**, 35 (2013).
 - [18] A. Carbone, A. Rios, and A. Polls, *Phys. Rev. C* **88**, 044302 (2013).
 - [19] G. Hagen, T. Papenbrock, A. Ekström, K. Wendt, G. Baardsen, S. Gandolfi, M. Hjorth-Jensen, and C. J. Horowitz, *Phys. Rev. C* **89**, 014319 (2014).
 - [20] M. Kohno, *Phys. Rev. C* **88**, 064005 (2013).
 - [21] F. Isaule, H. F. Arellano, and A. Rios, *Phys. Rev. C* **94**, 034004 (2016).
 - [22] A. Gezerlis, I. Tews, E. Epelbaum, S. Gandolfi, K. Hebeler, A. Nogga, and A. Schwenk, *Phys. Rev. Lett.* **111**, 032501 (2013).
 - [23] G. Wlazowski, J. W. Holt, S. Moroz, A. Bulgac, and K. J. Roche, *Phys. Rev. Lett.* **113**, 182503 (2014).
 - [24] A. Roggero, A. Mukherjee, and F. Pederiva, *Phys. Rev. Lett.* **112**, 221103 (2014).
 - [25] J. E. Lynn, I. Tews, J. Carlson, S. Gandolfi, A. Gezerlis, K. E. Schmidt, and A. Schwenk, *Phys. Rev. Lett.* **116**, 062501 (2016).
 - [26] V. Bernard, E. Epelbaum, H. Krebs, and U.-G. Meißner, *Phys. Rev. C* **77**, 064004 (2008).
 - [27] V. Bernard, E. Epelbaum, H. Krebs, and U.-G. Meißner, *Phys. Rev. C* **84**, 054001 (2011).
 - [28] I. Tews, T. Krüger, K. Hebeler, and A. Schwenk, *Phys. Rev. Lett.* **110**, 032504 (2013).
 - [29] T. Krüger, I. Tews, K. Hebeler, and A. Schwenk, *Phys. Rev. C* **88**, 025802 (2013).
 - [30] K. Hebeler, H. Krebs, E. Epelbaum, J. Golak, and R. Skibiński, *Phys. Rev. C* **91**, 044001 (2015).
 - [31] K. Hebeler, *Phys. Rev. C* **85**, 021002(R) (2012).
 - [32] K. Hebeler and R. J. Furnstahl, *Phys. Rev. C* **87**, 031302 (2013).
 - [33] R. Skibiński, J. Golak, K. Topolnicki, H. Witała, E. Epelbaum, W. Glöckle, H. Krebs, A. Nogga, and H. Kamada, *Phys. Rev. C* **84**, 054005 (2011).
 - [34] J. Golak, R. Skibiński, K. Topolnicki, H. Witała, E. Epelbaum, H. Krebs, H. Kamada, U.-G. Meißner, V. Bernard, P. Maris, J. Vary, S. Binder, A. Calci, K. Hebeler, J. Langhammer, R. Roth, A. Nogga, S. Liebig, and D. Minossi, *Eur. Phys. J. A* **50**, 177 (2014).
 - [35] N. Kaiser, *Eur. Phys. J. A* **48**, 135 (2012).
 - [36] K. Hebeler and A. Schwenk, *Phys. Rev. C* **82**, 014314 (2010).
 - [37] J. W. Holt, N. Kaiser, and W. Weise, *Phys. Rev. C* **81**, 024002 (2010).
 - [38] A. Carbone, A. Rios, and A. Polls, *Phys. Rev. C* **90**, 054322 (2014).
 - [39] K. Hebeler, J. M. Lattimer, C. J. Pethick, and A. Schwenk, *Phys. Rev. Lett.* **105**, 161102 (2010).
 - [40] W. H. Dickhoff and C. Barbieri, *Prog. Part. Nucl. Phys.* **52**, 377 (2004).
 - [41] A. Rios, A. Polls, and I. Vidana, *Phys. Rev. C* **79**, 025802 (2009).
 - [42] V. Soma and P. Bozek, *Phys. Rev. C* **80**, 025803 (2009).
 - [43] A. Carbone, A. Cipollone, C. Barbieri, A. Rios, and A. Polls, *Phys. Rev. C* **88**, 054326 (2013).
 - [44] D. Ding, A. Rios, H. Dussan, W. H. Dickhoff, S. J. Witte, A. Carbone, and A. Polls, *Phys. Rev. C* **94**, 025802 (2016).
 - [45] D. R. Entem and R. Machleidt, *Phys. Rev. C* **68**, 041001(R) (2003).
 - [46] E. Epelbaum, W. Glöckle, and U.-G. Meißner, *Nucl. Phys. A* **747**, 362 (2005).
 - [47] H. Krebs, A. Gasparyan, and E. Epelbaum, *Phys. Rev. C* **85**, 054006 (2012).

- [48] E. Epelbaum, H. Krebs, and U.-G. Meißner, Eur. Phys. J. A **51**, 53 (2015).
- [49] K. Hebeler, J. M. Lattimer, C. J. Pethick, and A. Schwenk, Astrophys. J. **773**, 11 (2013).
- [50] I. Tews, S. Gandolfi, A. Gezerlis, and A. Schwenk, Phys. Rev. C **93**, 024305 (2016).
- [51] A. Dyhdalo, R. J. Furnstahl, K. Hebeler, and I. Tews, Phys. Rev. C **94**, 034001 (2016).
- [52] A. Ekström, G. R. Jansen, K. A. Wendt, G. Hagen, T. Papenbrock, B. D. Carlsson, C. Forssén, M. Hjorth-Jensen, P. Navrátil, and W. Nazarewicz, Phys. Rev. C **91**, 051301(R) (2015).
- [53] B. D. Carlsson, A. Ekström, C. Forssén, D. F. Strömberg, G. R. Jansen, O. Lilja, M. Lindby, B. A. Mattsson, and K. A. Wendt, Phys. Rev. X **6**, 011019 (2016).